

Control of a Synchronous Motor With an Inverter Integrated Rotor

Eunsoo Jung, *Student Member, IEEE*, Sungmin Kim, *Student Member, IEEE*,
Jung-Ik Ha, *Senior Member, IEEE*, and Seung-Ki Sul, *Fellow, IEEE*

Abstract—In this paper, a synchronous motor with an inverter integrated rotor (SMIR) is introduced, and its control scheme is proposed. This presents a new breed of synchronous motor in that it integrates an inverter inside the rotor. The basic operational principle and control strategies are discussed. Given these new strategies, the SMIR can be considered as a synchronous motor which changes its field according to the harmonic voltage of the stator inverter. The feasibility of the proposed structure of the drive system and its operation principle are evaluated through experimental results.

Index Terms—AC motors, brushless rotating machines, pulsewidth-modulated inverters, variable-speed drives.

I. INTRODUCTION

RECENTLY, a variety of electrical drive applications have been extended to home appliances, transportation, industries, and renewable energy systems. In particular, permanent-magnet synchronous machines are vigorously utilized due to their high level of efficiency. However, the use of these machines is threatened due to the increasing cost of the rare earth resources. Thus, alternatives are required.

Generally, wound-rotor synchronous machines are known to show high efficiency in a wide speed range through their direct control of the field flux. In this system, the field windings for the construction of the flux have to rotate along with the rotor. Therefore, they are connected to an external excitation circuit through slip rings and brushes. Unfortunately, these slip rings and brushes are associated with issues such as mechanical/electrical losses and poor durability. Furthermore, they occupy a large portion of the machine size while making no contribution to the output of the machine. This limits their applications to low-power-density systems.

By connecting the field windings to diodes, as shown in Fig. 1, various brushless self-excited synchronous motors [driven by pulsewidth-modulation (PWM) inverters] have been developed [2]–[6]. In these drive systems, additional magnetic fields rotating at speeds different from that of the main field in the stator need to be injected to supply excitation power to the

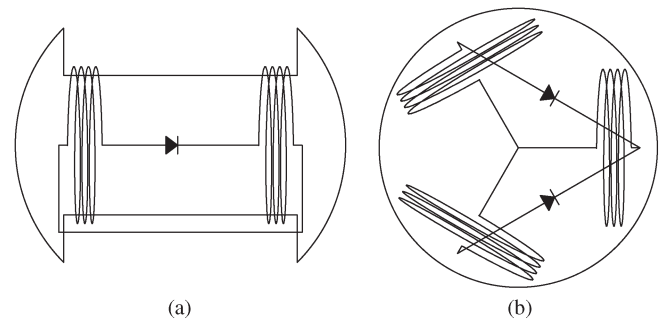


Fig. 1. Rotor structure of brushless self-excited synchronous motors. (a) Salient pole type. (b) Nonsalient pole type.

rotor [3]. However, because the field currents are obtained by rectifying the injected harmonic voltages, brushless self-excited synchronous motors require a sufficient amount of harmonic voltage. Accordingly, they generate a large torque ripple. To reduce the effect of the torque ripple, the injection frequency can be increased, but the magnitude of the field flux linkage and the efficiency of the power transfer decrease as a result of the increased levels of impedance.

In this paper, a synchronous motor with an inverter integrated rotor (SMIR) drive system is proposed. The integrated inverter is a voltage source inverter which consists of six switching devices. With these active switches in the rotor-side inverter, the rotor current can be controlled, and the torque control performance can be enhanced. Among the six switches, the three of them can be replaced with simple diodes due to the unidirectional current flow.

II. OPERATION PRINCIPLE OF THE SMIR

A. Structure of the SMIR

The structure of the proposed SMIR and its drive system are shown in Fig. 2. The stator is identical to that of an ordinary three-phase ac motor, and its windings are connected to a three-phase voltage source inverter. This is henceforth referred as a stator-side inverter.

On the other hand, the SMIR consists of a wound rotor. Its windings are connected to another rotor-side inverter which is included inside the rotor. Naturally, the rotor-side inverter rotates synchronously as the rotor rotates and is electrically isolated from the outside of the rotor. Therefore, the rotor-side inverter should be powered by means of electromagnetic coupling with the stator windings. A nonsalient pole type of rotor instead of salient pole type is considered in this paper because the balanced windings of the former lead to better operating performance.

Manuscript received January 13, 2012; revised May 12, 2012; accepted May 22, 2012. Date of publication October 23, 2012; date of current version December 31, 2012. Paper 2011-IDC-725.R1, approved for publication in the IEEE TRANSACTIONS ON INDUSTRY APPLICATIONS by the Industrial Drives Committee of the IEEE Industry Applications Society.

The authors are with Seoul National University, Seoul 151-742, Korea (e-mail: eunsoo@eepeel.snu.ac.kr; ksmin@eepeel.snu.ac.kr; jungikha@snu.ac.kr; sulsk@plaza.snu.ac.kr).

Color versions of one or more of the figures in this paper are available online at <http://ieeexplore.ieee.org>.

Digital Object Identifier 10.1109/TIA.2012.2226199

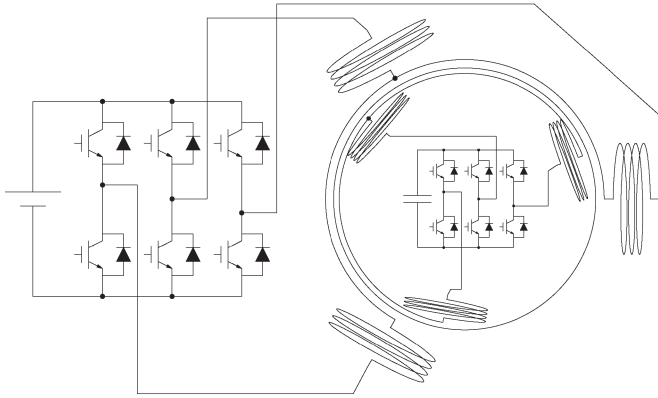
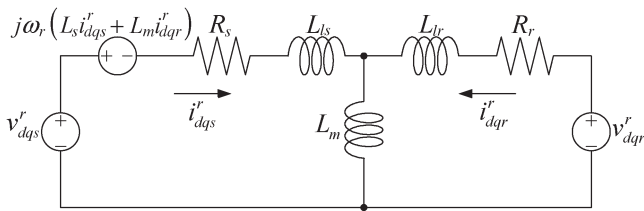


Fig. 2. Structure of the SMIIR drive system.

Fig. 3. Equivalent circuit in the d - q rotor reference frame.

B. Basic Operation Principle

An equivalent circuit of the SMIIR in the d - q rotor reference frame with complex vector notation is shown in Fig. 3 [7]. The voltage sources of v_{dqs}^r and v_{dqr}^r are the output voltages of the stator-side and the rotor-side inverters, respectively. From the circuit, the voltage equations are derived as

$$v_{dqs}^r = R_s i_{dqs}^r + \frac{d}{dt} (L_s i_{dqs}^r + L_m i_{dqr}^r) + j\omega_r (L_s i_{dqs}^r + L_m i_{dqr}^r) \quad (1)$$

$$v_{dqr}^r = R_r i_{dqr}^r + \frac{d}{dt} (L_r i_{dqr}^r + L_m i_{dqs}^r) \quad (2)$$

where $L_s = L_m + L_{ls}$ and $L_r = L_m + L_{lr}$.

It is clear that the fundamental components of both the stator and rotor currents have to be dc in the steady state for the motor to operate synchronously. Simultaneously, the rotor-side inverter has to supply constant power to handle the losses of the rotor circuit such as copper loss and switching loss and to power its controller. However, due to the absence of energy source in the rotor-side inverter, the dc-link voltage is fully dissipated. Thus, the rotor-side inverter eventually loses its controllability of the rotor current. Hence, the required amount of power should be supplied from the stator to the rotor so as to maintain the system.

As a means of transferring energy between the stator and rotor, ac components in the rotor reference frame can be considered for the electromagnetic coupling. In other words, if the stator-side inverter injects ac voltage at a different frequency from the fundamental component to the stator winding, this ac component appears in the rotor winding terminals according to the relationship between the stator and the rotor windings as a

transformer. To deal with the power delivered from the stator, an appropriate control scheme for the rotor-side inverter is needed with which the power transfer between the stator and rotor can be properly conducted.

C. Power Transfer to the Rotor

As the stator and the rotor have their own controllers, the stator current and the rotor currents can be controlled separately. High-frequency ac voltage, which is independent of the fundamental voltage, can be injected to the d - and q -axes in the rotor reference frame. Moreover, because the high-frequency components on the d - q -axes are independent, each axis can be regarded as a single-phase circuit.

Regarding the high-frequency ac voltages in stator- and rotor-side inverters, the output voltages of each type can be written as follows, respectively:

$$v_{ds}^r = v_{ds0}^r + v_{dsh}^r \quad (3)$$

$$v_{dr}^r = v_{dr0}^r + v_{drh}^r \quad (4)$$

where the subscripts 0 and h denote the dc component and the high-frequency ac component in the rotor reference frame for the fundamental current control and the power transfer from the stator to the rotor, respectively. Because the motor model is a linear system, the d -axis currents of the stator and rotor are also divided into dc and ac components, as expressed by the following, respectively:

$$i_{ds}^r = i_{ds0}^r + i_{dsh}^r \quad (5)$$

$$i_{dr}^r = i_{dr0}^r + i_{drh}^r. \quad (6)$$

Although the high-frequency components can be arbitrarily plural, a single frequency of ω_h is considered in this paper. For the analysis of the high-frequency ac component in a steady state, the voltage equation can be expressed in phasor term

$$\mathbf{V}_{dsh}^r = (jX_s + R_s)\mathbf{I}_{dsh}^r + jX_m\mathbf{I}_{drh}^r \quad (7)$$

$$\mathbf{V}_{drh}^r = jX_m\mathbf{I}_{dsh}^r + (jX_r + R_r)\mathbf{I}_{drh}^r. \quad (8)$$

Here, the bold capital letters denote the phasor variables, while X denotes the reactance at the ω_h frequency. From the phasor equations, the power transferred to the rotor-side inverter can be written as

$$\begin{aligned} P_{rd} &= -\frac{3}{2} \frac{1}{2} \text{Re} \left(\mathbf{V}_{drh}^r \bar{\mathbf{I}}_{drh}^r \right) \\ &= -\frac{3}{2} \frac{1}{2} \left(\text{Re} \left(\frac{X_m}{X_s - jR_s} \mathbf{V}_{dsh}^r \bar{\mathbf{I}}_{drh}^r \right) \right. \\ &\quad \left. + \left(\frac{X_m^2}{X_s^2 + R_s^2} R_s + R_r \right) |\mathbf{I}_{drh}^r|^2 \right) \quad (9) \end{aligned}$$

where the scale $3/2$ is the coefficient from Park's magnitude-invariant transformation [7]. The symbol “ $-$ ” above the complex variable stands for the conjugate of the variable. Assuming

that $X_s \gg R_s$ at the ω_h frequency, the output power can be approximated by

$$P_{rd} \approx -\frac{3}{2} \frac{1}{2} \left(\frac{X_m}{X_s} \text{Re}(\mathbf{V}_{dsh}^r \bar{\mathbf{I}}_{drh}^r) + \left(\frac{X_m^2}{X_s^2} R_s + R_r \right) |\mathbf{I}_{drh}^r|^2 \right). \quad (10)$$

The first term on the right-hand side denotes the power transfer from the stator to the rotor due to the high-frequency ac components, and the second term represents the additional copper loss due to the additional ac component current for the power transfer.

For the maximum power transfer per unit of ac current, the phase difference between the stator voltage and the rotor current is set as follows:

$$\angle \mathbf{V}_{dsh}^r - \angle \mathbf{I}_{drh}^r = \pi. \quad (11)$$

The power equation becomes

$$P_{rd} \approx \frac{3}{2} \frac{1}{2} \left(\frac{X_m}{X_s} |\mathbf{V}_{dsh}^r| |\mathbf{I}_{drh}^r| - \left(\frac{X_m^2}{X_s^2} R_s + R_r \right) |\mathbf{I}_{drh}^r|^2 \right). \quad (12)$$

In a similar way, the power transferred to the rotor on the q -axis can be obtained via

$$P_{rq} \approx \frac{3}{2} \frac{1}{2} \left(\frac{X_m}{X_s} |\mathbf{V}_{qsh}^r| |\mathbf{I}_{qrh}^r| - \left(\frac{X_m^2}{X_s^2} R_s + R_r \right) |\mathbf{I}_{qrh}^r|^2 \right). \quad (13)$$

The total power transferred to the rotor-side inverter is then determined through

$$P_r \approx \frac{3}{4} \left\{ \frac{X_m}{X_s} (|\mathbf{V}_{dsh}^r| |\mathbf{I}_{drh}^r| + |\mathbf{V}_{qsh}^r| |\mathbf{I}_{qrh}^r|) - \left(\frac{X_m^2}{X_s^2} R_s + R_r \right) (|\mathbf{I}_{drh}^r|^2 + |\mathbf{I}_{qrh}^r|^2) \right\}. \quad (14)$$

Because the power to the rotor determines the dc-link voltage of the rotor-side inverter, the dc-link voltage of the rotor can be controlled by adjusting the rotor current in antiphase with the injected stator voltage.

D. Voltage Injection Strategy

The maximum output voltage of the inverter is limited by its dc-link voltage. Therefore, the output voltage increment resulting from a high-frequency voltage injection has to be minimized to ensure the maximum level of fundamental voltage.

Instantaneous output voltages of the stator-side inverter can be written in complex vector expression as

$$v_{dq_s}^r = (v_{ds0}^r + v_{dsh}^r) + j(v_{qs0}^r + v_{qsh}^r). \quad (15)$$

The high-frequency voltage on the d - q -axes can be written as

$$\begin{aligned} v_{dsh}^r &= V_{dsh}^r \sin \omega_h t \\ v_{qsh}^r &= V_{qsh}^r \sin(\omega_h t + \delta) \end{aligned} \quad (16)$$

where δ denotes the phase difference between the two high-frequency voltages.

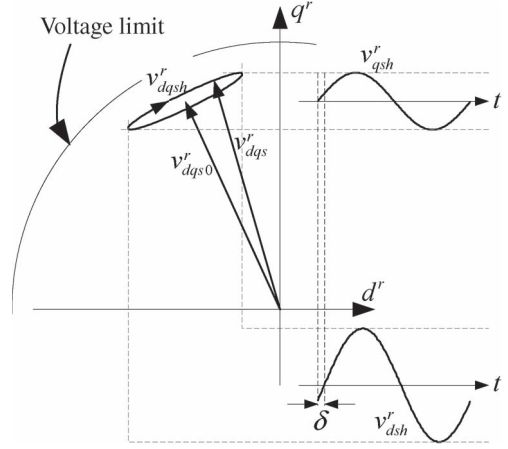


Fig. 4. Trajectory of the stator voltage in the d - q rotor reference frame.

The trajectory of the stator voltage in the d - q rotor reference frame is shown in Fig. 4 for physical intuition. As the motor operates, the fundamental voltage vector $v_{dq_s0}^r$ is located in the second quadrant, and the high-frequency voltage is added to the fundamental voltage vector, as shown in Fig. 4.

If high-frequency voltage is injected along the fundamental voltage vector, the peak output voltage increases according to the magnitude of the high-frequency voltage. To suppress the increment of the output voltage, the high-frequency voltage should be excited along the axis orthogonal to the fundamental voltage vector while satisfying

$$v_{ds0}^r V_{dsh}^r + v_{qs0}^r V_{qsh}^r = 0. \quad (17)$$

Moreover, because the thickness of the high-frequency voltage ellipse in Fig. 4 is proportional to $\sin \delta$, the phase difference between two high-frequency voltages has to be kept as small as possible. This being the case, for a simple development, it is assumed that

$$\sin \delta \ll 1. \quad (18)$$

Then, the high-frequency voltage ellipse can be regarded as a line orthogonal to the fundamental voltage vector.

E. Torque Ripple Suppression Method

During the operation of the motor, the stator and the rotor currents have to oscillate with the frequency of the injected voltage for power transfer. Because the motor torque is determined by the stator and rotor currents, the torque ripple from the high-frequency injection has to be considered. The torque equation of the motor can be expressed as

$$T_e = \frac{3}{2} \frac{P}{2} L_m (i_{dr}^r i_{qs}^r - i_{qr}^r i_{ds}^r). \quad (19)$$

Assuming that the fundamental components exist on the d -axis of the rotor and the q -axis of the stator, the torque equation becomes

$$T_e = \frac{3}{2} \frac{P}{2} L_m ((i_{dr0}^r + i_{drh}^r) (i_{qs0}^r + i_{qsh}^r) - i_{qrh}^r i_{dsh}^r). \quad (20)$$

The torque equation (20) can be divided into three terms according to the characteristic of the frequency as follows:

$$T_e = \frac{3P}{2} \frac{L_m}{2} \left(\underbrace{i_{dr0}^r i_{qs0}^r}_{(a)} + \underbrace{i_{dr0}^r i_{qsh}^r + i_{drh}^r i_{qs0}^r}_{(b)} + \underbrace{i_{drh}^r i_{qsh}^r - i_{qrh}^r i_{dsh}^r}_{(c)} \right). \quad (21)$$

The first term (a) in (21) represents the fundamental dc component, and the second term (b) indicates the ac component of the ω_h frequency. The last term (c) represents a product of the two ac components of the ω_h frequency. Because the last term (c) is a product of two ac components, it can be decomposed into the dc component and the ac component of the $2\omega_h$ frequency.

Considering (11) and (16), the high-frequency ac component of the rotor current can be written as

$$\begin{aligned} i_{drh}^r &= -I_{drh}^r \sin \omega_h t \\ i_{qrh}^r &= -I_{qrh}^r \sin(\omega_h t + \delta). \end{aligned} \quad (22)$$

Under the assumption of $X_s \gg R_s$, the stator current can be approximated from (7) as

$$\begin{aligned} i_{dsh}^r &\approx I_{dsh}^r \sin(\omega_h t + \phi_d) \\ i_{qsh}^r &\approx I_{qsh}^r \sin(\omega_h t + \delta + \phi_q) \end{aligned} \quad (23)$$

where $I_{dsh}^r = (1/X_s) \sqrt{(X_m I_{drh}^r)^2 + V_{dsh}^r{}^2}$, $\phi_d = -\tan^{-1}(V_{dsh}^r / X_m I_{drh}^r)$ and $I_{qsh}^r = (1/X_s) \sqrt{(X_m I_{qrh}^r)^2 + V_{qsh}^r{}^2}$, $\phi_q = -\tan^{-1}(V_{qsh}^r / X_m I_{qrh}^r)$.

Substituting (22) and (23) for (21), each term of the torque equation (21) becomes

$$\begin{aligned} (a) &= i_{dr0}^r i_{qs0}^r \\ (b) &= -i_{qs0}^r I_{drh}^r \sin \omega_h t + i_{dr0}^r I_{qsh}^r \sin(\omega_h t + \delta + \phi_q) \\ (c) &= -I_{drh}^r I_{qsh}^r \sin \omega_h t \sin(\omega_h t + \delta + \phi_q) \\ &\quad + I_{qrh}^r I_{dsh}^r \sin(\omega_h t + \delta) \sin(\omega_h t + \phi_d). \end{aligned} \quad (24)$$

The torque ripple (b) of the ω_h frequency can be canceled out under the following conditions:

$$\frac{I_{qsh}^r}{i_{qs0}^r} = \frac{I_{drh}^r}{i_{dr0}^r} \quad \delta = -\phi_q. \quad (25)$$

With the conditions of (25), the third term (c) of the torque equation is determined as

$$\begin{aligned} (c) &= -\frac{1}{2} I_{drh}^r I_{qsh}^r + I_{qrh}^r I_{dsh}^r \frac{\cos(\phi_d + \phi_q)}{2} \\ &\quad + I_{drh}^r I_{qsh}^r \frac{\cos 2\omega_h t}{2} - I_{qrh}^r I_{dsh}^r \frac{\cos(2\omega_h t + \phi_d - \phi_q)}{2}. \end{aligned} \quad (26)$$

Moreover, if $\phi_d = \phi_q$, which means that the vector of the high-frequency voltage excitation is coincident with the vector

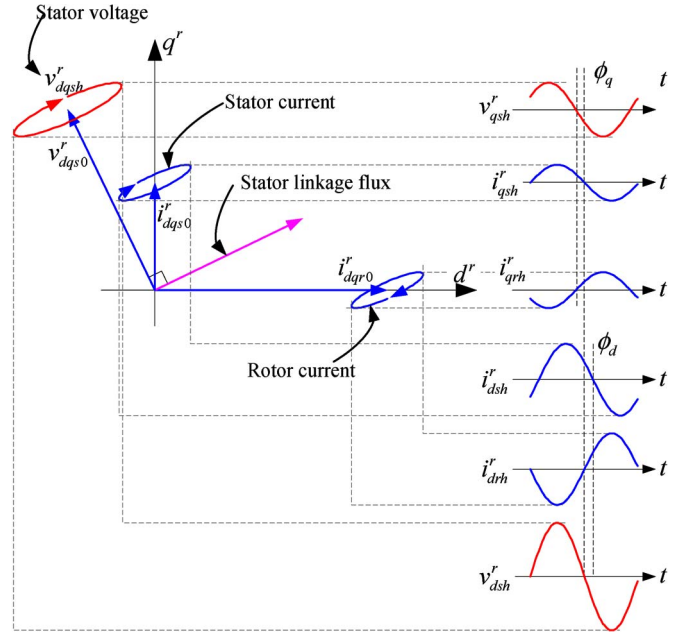


Fig. 5. Stator and rotor currents in the d - q rotor reference frame.

of the high-frequency current oscillation, the magnitudes of the high-frequency stator currents become

$$\begin{aligned} I_{dsh}^r &= \frac{X_m}{X_s} \sqrt{1 + k^2} I_{drh}^r \\ I_{qsh}^r &= \frac{X_m}{X_s} \sqrt{1 + k^2} I_{qrh}^r \end{aligned} \quad (27)$$

where $k = V_{dsh}^r / X_m I_{drh}^r = V_{qsh}^r / X_m I_{qrh}^r$.

Equation (26) can then be simplified to

$$(c) = -I_{dsh}^r I_{qrh}^r \frac{k^2}{1 + k^2}. \quad (28)$$

Finally, the torque equation becomes

$$T_e = \frac{3P}{2} \frac{L_m}{2} \left(i_{dr0}^r i_{qs0}^r - I_{dsh}^r I_{qrh}^r \frac{k^2}{1 + k^2} \right). \quad (29)$$

In (29), the magnitude of the second term is much smaller than that of the first term because each high-frequency component is smaller than the fundamental component and k is less than one. Practically, the second term is neglected.

Fig. 5 shows the current trajectories of the stator and the rotor according to the voltage injection strategy and the torque ripple suppression method to provide a physical understanding. The figure shows that the stator and the rotor currents oscillate along the direction of the stator linkage flux vector in the rotor reference frame.

III. CONTROL OF THE PROPOSED MOTOR

A. Stator-Side Control Scheme

In the proposed SMIIR drive system, the stator-side inverter has two main functions: the stator current control and the power transfer into the rotor via a high-frequency voltage injection. A block diagram of the stator current controller is shown in Fig. 6. The stator current controller is based on the synchronous

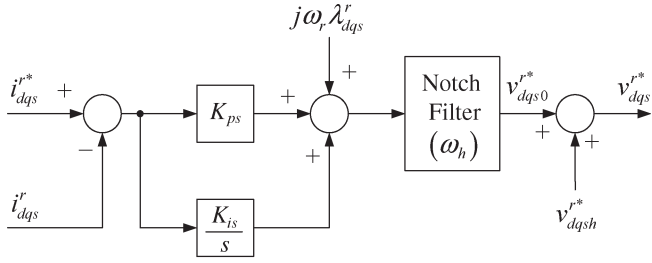


Fig. 6. Control block diagram of the stator current controller.

reference frame proportional and integral (PI) controller. A narrow notch filter was added to the controller output to limit the interference between the stator- and rotor-side controllers at the ω_h frequency. The output of the fundamental current controller can be depicted as

$$v_{ds0}^{r*} = \text{Notch} \left\{ K_{ps} (i_{ds}^{r*} - i_{ds}^r) + K_{is} \int (i_{ds}^{r*} - i_{ds}^r) dt - \omega_r \lambda_{qs}^r \right\}$$

$$v_{qs0}^{r*} = \text{Notch} \left\{ K_{ps} (i_{qs}^{r*} - i_{qs}^r) + K_{is} \int (i_{qs}^{r*} - i_{qs}^r) dt + \omega_r \lambda_{ds}^r \right\} \quad (30)$$

where $\text{Notch}\{\}$ refers to the notch filter, of which the stop frequency is ω_h applied to the variables inside of $\{\}$. K_{ps} and K_{is} represent the proportional and integral gains, respectively. The gains of the current controller can be set to $K_{ps} = \sigma L_s \omega_{cs}$ and $K_{is} = (R_s + R_r L_m^2 / L_s^2) \omega_{cs}$.

The high-frequency voltages which satisfy condition (17) can be derived as

$$v_{dsh}^{r*} = \frac{-v_{ds0}^r}{\sqrt{v_{ds0}^{r*2} + v_{qs0}^{r*2}}} V_{inj} \sin \omega_h t$$

$$v_{qsh}^{r*} = \frac{v_{qs0}^r}{\sqrt{v_{ds0}^{r*2} + v_{qs0}^{r*2}}} V_{inj} \sin(\omega_h t + \delta) \quad (31)$$

where V_{inj} is the magnitude of the injected high-frequency voltage. The total voltage reference for the stator-side inverter is then determined as follows:

$$v_{dqs}^{r*} = v_{dqs0}^{r*} + v_{dqs}^{r*} \quad (32)$$

B. Rotor-Side Control Scheme

The rotor-side controller consists of a dc-link voltage regulator, a current controller, and a stator voltage observer, as shown in Fig. 7.

1) *DC-Link Voltage Regulation:* The rotor-side inverter has no energy source but does have a small dc-link capacitor. Thus, this dc-link voltage has to be regulated to control the rotor current. According to the voltage injection strategy and the torque ripple suppression method previously mentioned, the high-frequency current reference i_{dqrh}^{r*} is determined by the stator voltage v_{dqs}^r through the relationship of $k = V_{dsh}^r / X_m I_{drh}^r = V_{qsh}^r / X_m I_{qrh}^r$. This means that the magnitude of the average

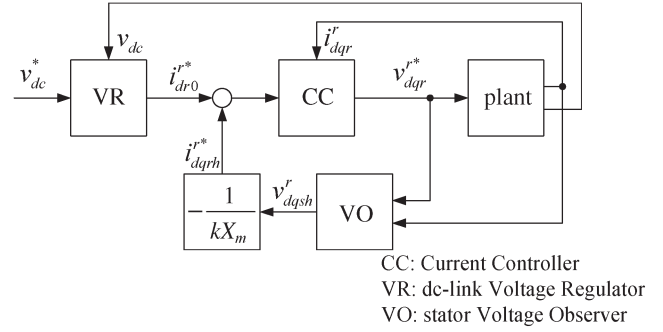


Fig. 7. Structure of the rotor-side controller.

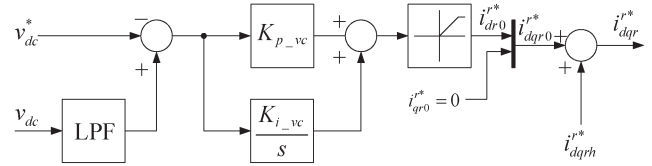


Fig. 8. Structure of the dc-link voltage regulator.

power transfer is also determined by the magnitude of the stator voltage as expressed by (14).

The purpose of the power transfer is to handle the power losses in the rotor circuit, including the integrated inverter. Thus, if the transferred power is greater than the losses, the excess can be balanced by increasing the field current to maintain the dc-link voltage. A block diagram of the dc-link voltage regulator is shown in Fig. 8. The field current reference can be written as the output of the dc-link voltage regulator

$$I_{dr0}^{r*} = - \left(K_{p_vc} + \frac{K_{i_vc}}{s} \right) (V_{dc}^* - \text{LPF}(V_{dc})) \quad (33)$$

where K_{p_vc} and K_{i_vc} are the proportional and integral gains of the voltage regulator, respectively. $\text{LPF}(\cdot)$ denotes a low-pass filter to suppress the periodic voltage ripple due to the reactive power during the power transfer. Because it is assumed that the field current exists only on the rotor d -axis, i_{qr0}^{r*} is always zero. The summation of the field current and the high-frequency reference then becomes the total current reference of the rotor current controller.

2) *Current Control:* The rotor-side inverter has to control the dc current for the field flux and the high-frequency current to receive adequate power from the stator. DC current control can be achieved simply through the use of a PI controller. However, it is difficult to control the high-frequency current with a PI controller due to the phase delay. To deal with the phase error, two separate PI controllers can be utilized for the positive sequence and the negative sequence. This structure is shown to be equivalent to a resonant controller [8]. Accordingly, the output voltage of the rotor current controller can be written in the frequency domain as

$$V_{dqr}^{r*} = \left(K_{pr} + \frac{K_{ir}}{s} + \frac{K_{rr}s}{s^2 + \hat{\omega}_h^2} \right) (I_{dqr}^{r*} - I_{dqr}^r) \quad (34)$$

where $K_{pr} = \sigma L_r \omega_{cr}$, $K_{ir} = (R_r + R_s L_m^2 / L_r^2) \omega_{cr}$, and $K_{rr} = \sigma L_r \omega_h \omega_{cr}$ represent the proportional, integral, and

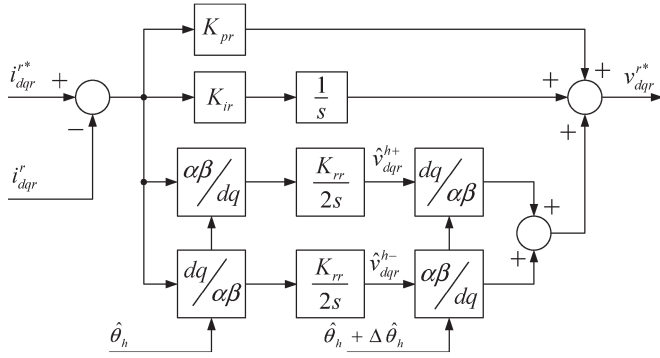


Fig. 9. Structure of the rotor current controller.

resonant gains, respectively. $\hat{\omega}_h$ denotes the estimated frequency of the injected stator voltage. The structure of the rotor current controller is shown in Fig. 9.

3) *Stator Voltage Estimation*: For the appropriate operation of the resonant controller, the frequency of the stator voltage should be identified. Moreover, the magnitude and phase of the stator voltage are required to keep the ratio between the stator voltage and the rotor current as a given constant, denoted here as k . If there is no communication between the stator- and rotor-side inverters, which is the case considered in this paper, information about the stator voltage has to be estimated.

From the voltage equations, the transfer function of the plant model can be obtained as follows:

$$I_{dqr}^r = \frac{L_s s + R_s}{\sigma L_r L_s s^2 + (L_s R_r + L_r R_s) s + R_s R_r} \times \left(V_{dqr}^r - \frac{L_m s}{L_s s + R_s} V_{dqs}^r \right). \quad (35)$$

Here, $\sigma = 1 - (L_m^2/L_s L_r)$ denotes the leakage coefficient.

As the transfer function of the system is complex, it is difficult to design an observer. Fortunately, because the variable of interest is the high-frequency voltage, the system model can be approximated near the injected frequency ω_h , where $L_s s$ is much larger than R_s . The simplified plant model can then be written as a first-order system

$$I_{dqr}^r = \frac{1}{\sigma L_r s + \left(R_r + \frac{L_r}{L_s} R_s \right)} \left(V_{dqr}^r - \frac{L_m}{L_s} V_{dqs}^r \right). \quad (36)$$

Based on this approximated model, a stator voltage observer was designed as shown in Fig. 10. The structure of the feedback observer is identical to that of the rotor current controller

$$V_{dqr}^r = \left(K_{po} + \frac{K_{io}}{s} + \frac{K_{ro} s}{s^2 + \hat{\omega}_h^2} \right) \left(I_{dqr}^r - \hat{I}_{dqr}^r \right) + V_{dqr}^{r*} \quad (37)$$

where K_{po} , K_{io} , and K_{ro} denote the proportional, integral, and resonant gains of the observer, respectively. \hat{I}_{dqr}^r denotes the estimated rotor current. Because the resonant term in (37) has infinite gain at the frequency of $\hat{\omega}_h$, it offsets the error when the frequency is near $\hat{\omega}_h$. Assuming that all of the parameters are known, this compensating voltage can be regarded as the stator voltage scaled by $-(L_m/L_s)$ according to (36).

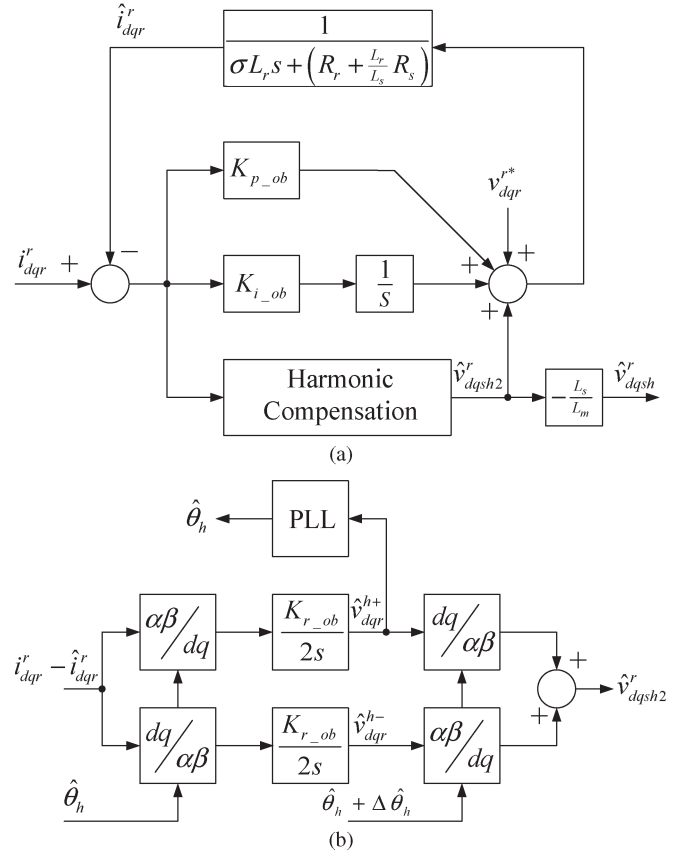


Fig. 10. Structure of the stator voltage observer. (a) Stator voltage observer. (b) Harmonic compensator for high-frequency component.

IV. EXPERIMENTAL RESULTS

Experiments were performed to verify the feasibility of the proposed SMIIR and its control method. The experimental setup is shown in Fig. 11. The system consists of a test motor and two three-phase inverters for the stator and the rotor, respectively. An industrial standard wound-rotor induction motor is used as the test motor. It is coupled to a load machine for the test of the load torque. The specification of the test motor is listed in Table I. The stator-side inverter is powered by a diode rectifier of which the dc-link voltage is 310 V. It is controlled by one DSP control board. On the other hand, the rotor-side inverter has no external power source. It is controlled by another DSP board.

At the beginning of the motor operation, because there is no voltage in the rotor dc link, it has to be charged by the stator-side inverter, as shown in Fig. 12. As the stator-side inverter injects voltages of 500 Hz, the rotor dc-link capacitor is charged by the diode rectification of the rotor-side inverter (Table II). When the dc-link voltage reaches 40 V, the rotor-side controller starts to work.

When the rotor-side controller starts, the rate of the dc-link voltage change is close to zero, as shown in Fig. 12(b). This occurs because the stator voltage observer and the phase locked loop are not stabilized during the power-up process. If the estimated stator voltage is not exact, the power flow is unexpected because the rotor current reference is derived from the estimation. After the stabilization of the voltage observer,

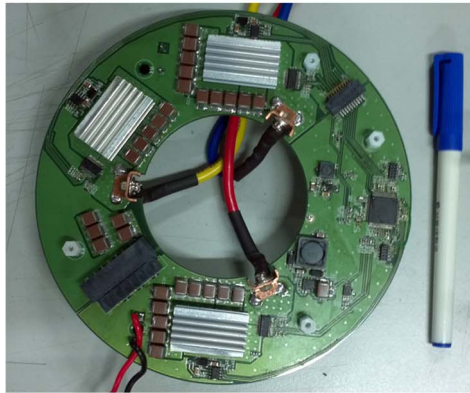
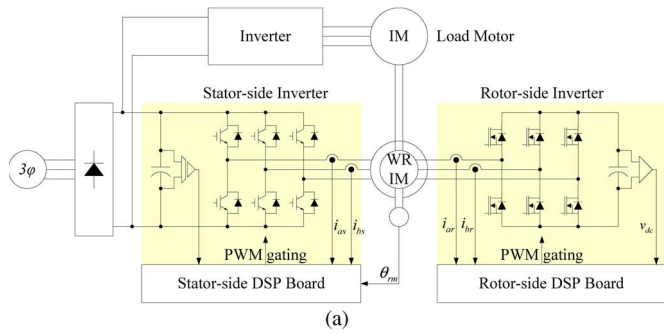


Fig. 11. Experimental setup. (a) Experimental setup. (b) Rotor-side inverter. (c) Test motor; wound-rotor induction motor.

TABLE I
SPECIFICATION OF THE TEST MOTOR*

Type	Wound Rotor Induction Motor		
Standard	IEC 34	No. of Pole	6
Rated Power	9 kW (60%ED)	Rated Speed	1165 r/min
Rated Sator Current	44.2 A _{rms}	Rated Rotor Current	25.3 A _{rms}
Rated Sator Voltage	220 V _{rms}	Magnetizing Inductance*	14.3 mH
Sator Inductance	15.3 mH	Rotor Inductance*	15.3 mH
Sator Resistance	0.09 Ω	Rotor Resistance*	0.09 Ω
Inertia	0.4 kg.m ²		

* Referred to the stator-side

the dc-link voltage is charged again rapidly by the power from the injected voltage and the synchronized rotor current. It is apparent that the dc component of the rotor current increases as the dc-link voltage exceeds the voltage reference of 70 V. The

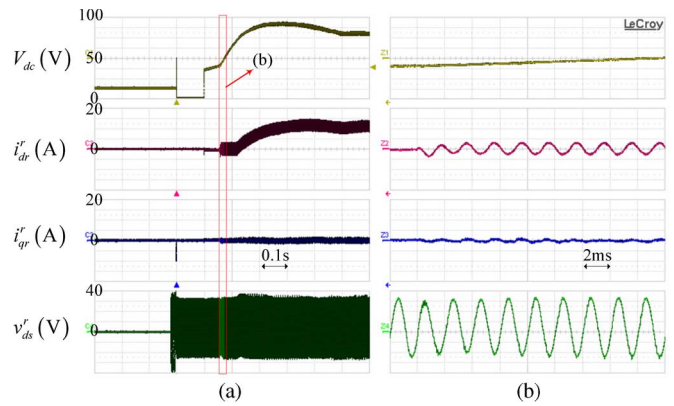


Fig. 12. Initial rotor capacitor charging operation. (a) Entire view. (b) Enlarged view.

TABLE II
SPECIFICATIONS OF THE ROTOR-SIDE INVERTER

DC capacitor	2.5mF	DC voltage	50~90V
Device	MOSFET	Diameter	160mm
Inertia(expected)	~5 g.m ²		

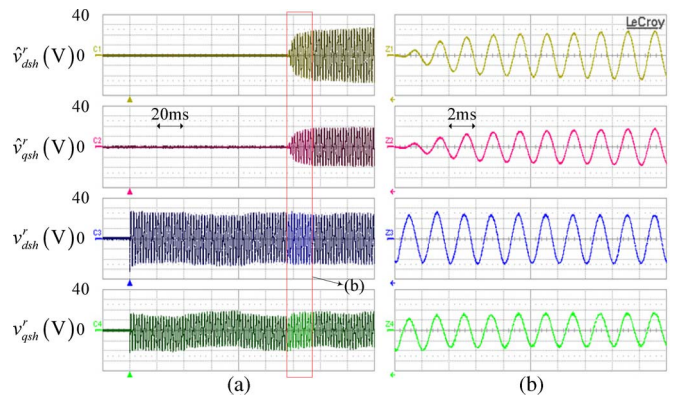


Fig. 13. Stator voltage and the estimated stator voltage.

dc-link voltage then settles down as the transferred power and rotor losses are balanced out.

Fig. 13 shows the performance of the stator voltage observer. The waveform in Fig. 13(a) represents the estimated stator voltage upon the start of the rotor-side controller, and Fig. 13(b) shows the estimated stator voltage in a steady state. According to Fig. 13, the estimated stator voltage tracks the actual value with accuracy except a small amount of error on *d*-axis in Fig. 13(b). This error appears to stem from the nonlinearity of the stator-side inverter.

It would be possible to enhance the estimation accuracy by offsetting the nonlinearity of the inverter or the imbalance in the plant model. However, the enhancement is not considered because the estimation error is acceptable in this case.

To determine the torque ripple characteristic under the torque ripple suppression method, the test motor is driven to generate constant torque. Fig. 14 shows the waveforms of the stator and rotor currents when the torque reference is 18 N · m and the

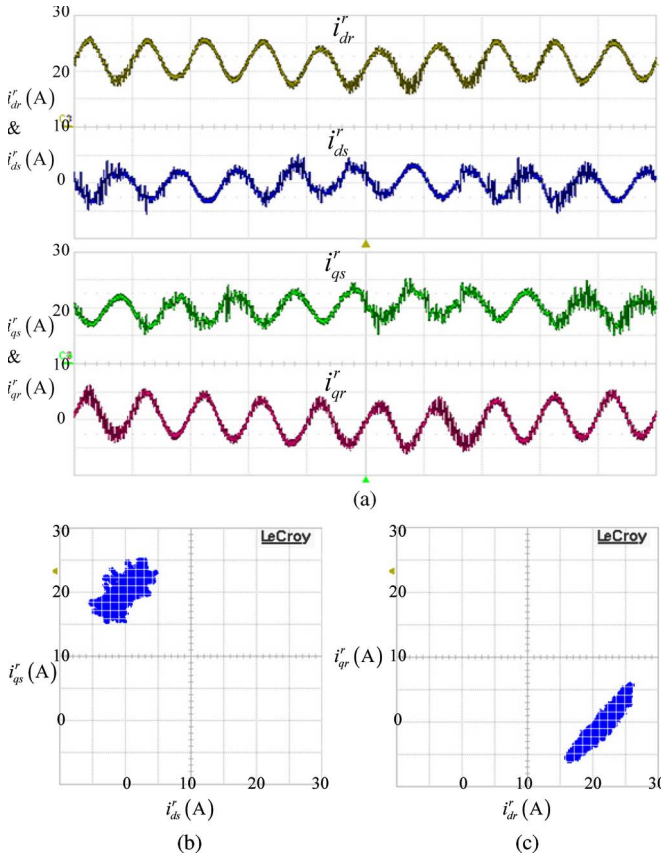


Fig. 14. Stator and rotor current trajectories at 1400 r/min. (a) Stator and rotor current. (b) Stator current trajectory. (c) Rotor current trajectory.

rotating speed is 1400 r/min. For the torque ripple suppression method, $k = V_{dsh}^r / X_m I_{dsh}^r$ is set to 0.12 so that the magnitudes of the high-frequency voltage and the current have the same per-unit value. The stator and rotor currents have to be opposite from the phase difference of $\delta = -0.12$ rad.

The stator and rotor currents in Fig. 14 are shown to be controlled well because they are in antiphase to each other and because they oscillate in the same direction formed by the fundamental stator current and the dc rotor current. However, the phase difference δ cannot be recognized because it is too small.

In general, the torque ripple of the motor can be directly measured by a torque sensor or indirectly estimated from the ripple of the angular speed. However, if the frequency of the torque ripple is too high, it is difficult to identify the torque ripple as a consequence of the filtering effect of inertia. As the torque ripple of the test motor mainly has the frequency of the injected voltage, it is not directly measurable. Thus, the torque ripple is calculated with the stator and rotor currents based on the torque equation. The result of the calculation reveals that the torque is nearly constant in spite of the high ratio of ac current to dc current.

Fig. 15 shows the experimental results of the stator output voltage under the same condition shown in Fig. 14. The rotor current and the stator voltage are opposite from each other for the power transfer. The figure shows that the high-frequency voltage oscillates in a direction orthogonal to the fundamental

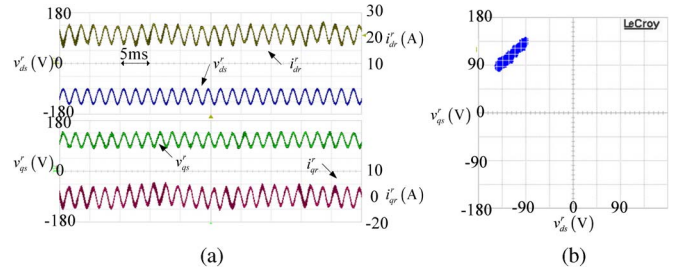


Fig. 15. Stator output voltage trajectory at 1400 r/min. (a) Stator output voltage in the $d-q$ frame. (b) Trajectory of the stator voltage.

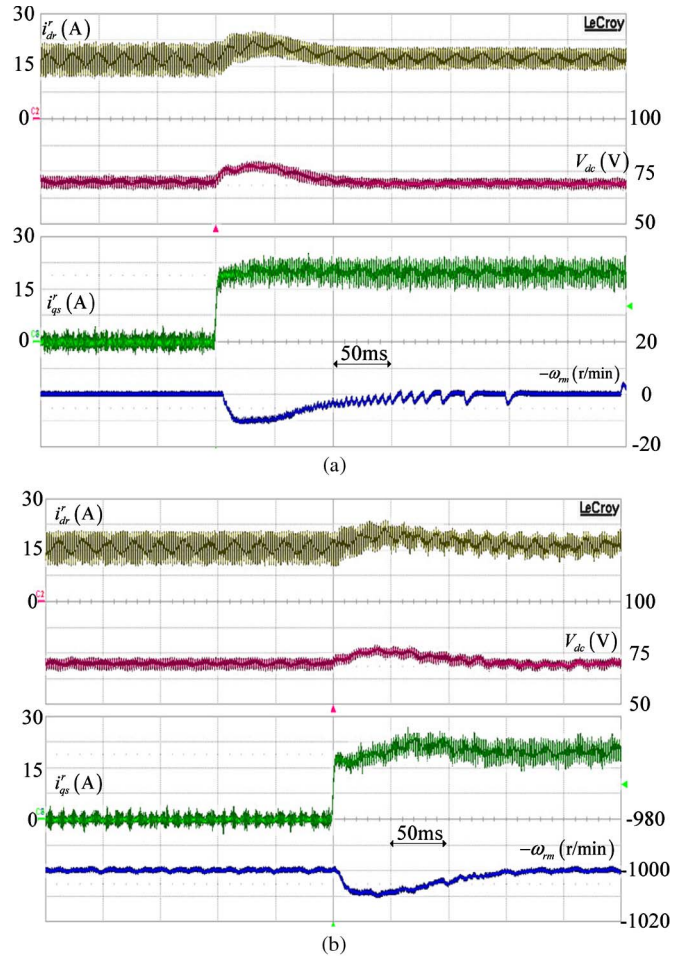


Fig. 16. Torque step reference. (a) Operation at standstill. (b) Operation at -1000 r/min.

voltage vector to suppress the increment of the output voltage due to the high-frequency voltage injection.

Fig. 16 shows the step response of the test motor. At standstill and near the rated speed, the torque reference changes from 0 to 20 A. The rising time of the torque response is similar to that of 200-Hz first-order low-pass filters. To guarantee the torque response, the bandwidth of the q -axis controller of the rotor-side inverter has been set to 10 Hz, which is 1/20 of the bandwidth of the stator-side q -axis controller. The q -axis rotor controller acts as a small resistor except near the injected frequency. As a result, the closed-loop performance of the stator-side inverter is nearly identical to the case of the rotor-side inverter short.

V. CONCLUSION

An SMIIR driven with two PWM inverters has been introduced in this paper. It is a new breed of synchronous motor which has semiconductors as a part of the motor. The rotor-side inverter is powered by a high-frequency voltage injection of the stator-side inverter. The rotor current, which builds up the field flux, can be adjusted by changing of the magnitude of the injection voltage. Thus, the SMIIR can be considered as a synchronous motor that changes its field according to the harmonic voltage of the stator.

Due to the high-frequency voltage injection, the effective output voltage of the stator inverter for the fundamental component can be reduced. The increment of the inverter output voltage to synthesize the high-frequency voltage can be kept as small as possible through the use of the proposed voltage injection strategy. In addition, a control method to suppress the torque ripple due to the high-frequency voltage has been proposed, and an equation representing the ripple torque has been derived. The experimental results confirm the suppression of torque ripple and the concurrent maintenance of the dc-link voltage of the rotor inverter. The feasibility of the SMIIR drive system and its operation strategies were evaluated by experiment results.

REFERENCES

- [1] P. Kundur, *Power System Stability and Control*. New York: McGraw-Hill, 1993, p. 322.
- [2] S. Nonaka and K. Fujii, "Brushless self-excited three-phase synchronous motor driven by voltage source inverter," *Elect. Eng. Jpn.*, vol. 103, no. 4, pp. 81–89, Aug. 1983.
- [3] M. M. EL Missiry, "Excitation control of a brushless synchronous motor," *IEEE Trans. Ind. Appl.*, vol. IA-20, no. 5, pp. 1285–1289, Sep./Oct. 1984.
- [4] S. Nonaka and H. Takami, "Low-speed drive of PWM-VSI-fed brushless self-excited synchronous motor," *IEEE Trans. Ind. Appl.*, vol. IA-22, no. 5, pp. 847–848, Sep./Oct. 1986.
- [5] J. Oyama, T. Higuchi, T. Abe, and E. Yamada, "Analysis of half-wave rectified brushless synchronous motor with permanent magnets," in *Conf. Rec. IEEE IAS Annu. Meeting*, 1990, pp. 146–151.
- [6] S. Nonaka and T. Kawaguchi, "A new variable-speed ac generator system using a brushless self-excited-type synchronous machine," *IEEE Trans. Ind. Appl.*, vol. 28, no. 2, pp. 490–496, Mar./Apr. 1992.
- [7] S. K. Sul, *Control of Electric Machine Drive Systems*. Hoboken, NJ: Wiley, 2011.
- [8] D. N. Zmood and D. G. Holmes, "Stationary frame current regulation of PWM inverters with zero steady-state error," *IEEE Trans. Power Electron.*, vol. 18, no. 3, pp. 814–822, May 2003.



Eunsoo Jung (S'08) was born in Korea in 1983. He received the B.S. degree in mechanical and aerospace engineering from Seoul National University, Seoul, Korea, in 2005, where he is currently working toward the Ph.D. degree in electrical engineering and computer science.

His current research interests are electric machine drives and power-converter circuits.



Sungmin Kim (S'09) was born in Seoul, Korea, in 1980. He received the B.S. and M.S. degrees in electrical engineering from Seoul National University, Seoul, in 2002 and 2008, respectively, where he is currently working toward the Ph.D. degree.

His current research interests are power electronics, machine design and drives, sensorless drives, and power conversion circuits.



Jung-Ik Ha (S'97–M'01–SM'12) was born in Korea in 1971. He received the B.S., M.S., and Ph.D. degrees in electrical engineering from Seoul National University, Seoul, Korea, in 1995, 1997, and 2001, respectively.

From 2001 to 2002, he was a Researcher with Yaskawa Electric Company, Kitakyushu, Japan. From 2003 to 2008, he was a Senior and Principal Engineer with Samsung Electronics Company, Suwon, Korea. From 2009 to 2010, he was Chief Technology Officer with LS Mecapion Company, Daegu, Korea. Since 2010, he has been an Assistant Professor with the School of Electrical Engineering, Seoul National University. His research interests are in circuits and control in high-efficiency and integrated electric energy conversions for various industrial fields.



Seung-Ki Sul (S'78–M'80–SM'98–F'00) was born in Korea in 1958. He received the B.S., M.S., and Ph.D. degrees in electrical engineering from Seoul National University, Seoul, Korea, in 1980, 1983, and 1986, respectively.

From 1986 to 1988, he was an Associate Researcher with the Department of Electrical and Computer Engineering, University of Wisconsin, Madison. From 1988 to 1990, he was a Principal Research Engineer with Gold-Star Industrial Systems Company. Since 1991, he has been a Professor with the School of Electrical Engineering and Computer Science, Seoul National University, where he was the Vice Dean from 2005 to 2007 and was the President of the Korea Electrical Engineering and Science Research Institute from 2008 to 2011. His current research interests are power-electronic control of electric machines, electric/hybrid vehicle drives, and power-converter circuits.